

# Reports

## Dissociation Reaction in Forsterite Under Shock Compression

**Abstract.** *Transmission electron microscopic observation of forsterite ( $Mg_2SiO_4$ ) shocked to peak pressures of 78 to 92 gigapascals revealed that forsterite breaks down to an assemblage of MgO plus  $MgSiO_3$  glass. This strongly supports the interpretation that the high-pressure phase of forsterite under shock compression is due to the assemblage of  $MgSiO_3$  perovskite plus MgO.*

Shock compression (Hugoniot) data have been used to study the equation of state of materials at pressures as high as a few hundred gigapascals, and data on the constitution of the earth's lower mantle and core are largely derived from shock compression studies of earth materials (1). Since forsterite-rich olivine is an important mineral species in the earth's mantle, extensive shock compression studies of olivines and olivine rocks have been carried out (2, 3). Recent shock compression measurements of single-crystal forsterite (3) revealed that a phase transition took place above about 50 GPa and the high-pressure phase above 120 GPa could be due to a mixed-phase assemblage of  $MgSiO_3$  perovskite plus MgO. However, no evidence for such an extensive dissociation reaction was found in shock-recovered olivines, even at pressures well above the phase transition (4), and inconsistency between shock compression measurements and observations of the residual effects of shock has been a serious difficulty in the application of shock data to geophysical problems. In the work reported here, we examined shock-recovered forsterite under the transmission electron microscope (TEM) and found evidence for the dissociation reaction or possibly incongruent melting in olivine under dynamic compression.

Shock-loading experiments were carried out at peak pressures of 78 to 92 GPa, using a two-stage light gas gun 9 m long with a launcher 2 cm in diameter (5). Platelets of single-crystal forsterite 8 mm in diameter and 1 mm thick, grown by the Czochralski method (6), were sandwiched between two 1-mm-thick copper disks encased in a stainless steel container. Fragments of the shocked crystals were recovered from the backing copper plate in which they were embedded. Finely ground powders of the recovered

specimens were dispersed on the microgrid and examined by observing their TEM images and electron diffraction patterns, as well as characteristic x-ray energy dispersion spectra obtained by analytical TEM (7).

The TEM images revealed the coexistence of various degrees of disorder in the shocked crystals. They were, in order of increasing disorder, relatively undamaged crystals (Fig. 1), completely recrystallized polycrystalline forsterite, dissociation products of microcrystalline MgO plus glass (Fig. 2), and further differentiated glasses with nearly enstatite composition (Fig. 3).

Figure 2, a and b, shows the heterogeneous texture of shocked forsterite on the TEM scale. The electron diffraction pattern demonstrates the coexistence of brecciated crystals, recrystallized polycrystals, and glass. Most of the diffrac-

tion rings were explained by the reflections from polycrystalline forsterite. Spot reflections from crystals fell exactly on these ring patterns, confirming that the polycrystalline material was recrystallized forsterite. In addition to a remarkable halo due to glass, rather broad ring patterns (labeled by arrows in Fig. 2b) were identified as being due to reflections from MgO, indicating that a dissociation reaction took place under shock loading.

To confirm the dissociation reaction, we examined a spherule-like part without appreciable contrast on the margin of the aggregate (Fig. 2a) under higher magnification with 1000-kV TEM (Fig. 2, c and d). The electron diffraction pattern consisted solely of the broad ring patterns due to fine MgO precipitates (arrows in Fig. 2d) and the halo due to glass. The size of MgO precipitates was about several nanometers, consistent with the broad line width.

Chemical analysis of differentiated glasses in situ showed considerable loss of Mg relative to Si, indicating local differentiation within the submicrosecond time scale of the shock (compare Figs. 1c and 3c). The Mg/Si ratio in these glasses was found to vary from 0.8 to 1.3, suggesting that the mode of the dissociation under shock compression was



These TEM observations support the interpretation that the high-pressure phase of shocked forsterite is due to an assemblage of  $MgSiO_3$  perovskite plus MgO, as proposed by Jackson and Ah-

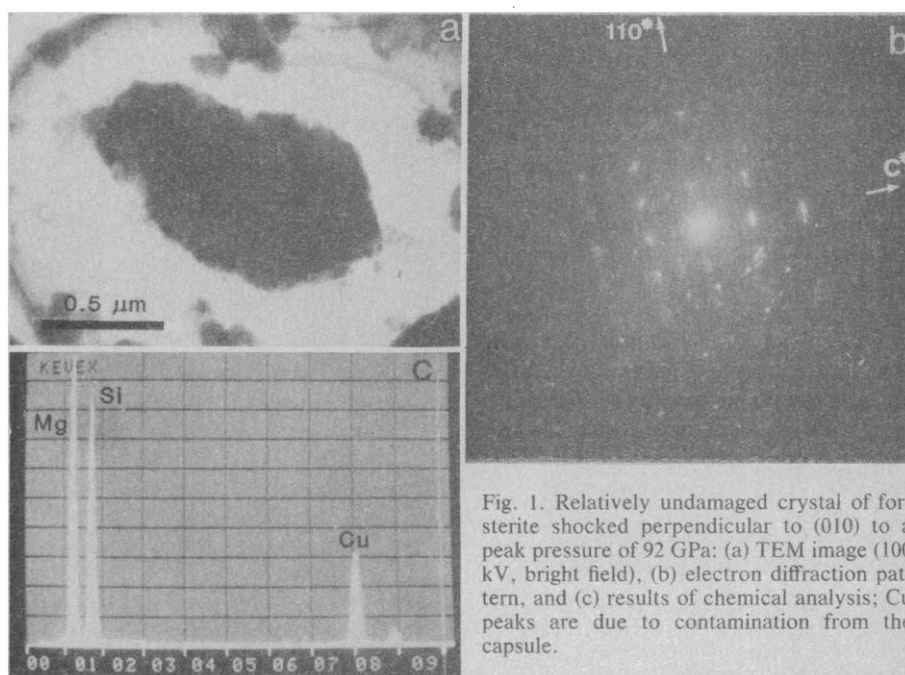


Fig. 1. Relatively undamaged crystal of forsterite shocked perpendicular to (010) to a peak pressure of 92 GPa: (a) TEM image (100 kV, bright field), (b) electron diffraction pattern, and (c) results of chemical analysis; Cu peaks are due to contamination from the capsule.

rens (3). Presumably, a dissociation of forsterite to  $\text{MgSiO}_3$  perovskite plus  $\text{MgO}$ , similar to the reaction established in static high-pressure experiments (8), takes place during shock compression. Glasses with compositions close to  $\text{MgSiO}_3$  might have been converted during the release process from the perovskite structure or perovskite-like randomized structure of shock-compressed states. Alternatively, our results could be due to incongruent melting, in which forsterite breaks down to  $\text{MgO}$  crystals plus  $\text{MgSiO}_3$  melt at the very high pres-

ures and temperatures produced by shock compression. This is also a likely explanation, since recent molecular dynamics calculations for silicate melts (9) indicate that  $\text{Mg}_2\text{SiO}_4$  melt becomes energetically unstable relative to crystalline  $\text{MgO}$  plus  $\text{MgSiO}_3$  melt at high pressures. The local structure of  $\text{MgSiO}_3$  melt at high pressures is also considered similar to the perovskite structure (9).

The complex textures observed in shocked forsterite are compatible with the current heterogeneous yielding model for brittle substances with low thermal

conductivity (10). Stress is concentrated in the sheared region, where the temperature is high enough for melting or thermal activation of reconstructive-type phase transformations, while the state of material between the sheared zones should differ little from that achieved by static compression and this material should remain relatively undamaged. This explanation applies not only to the heterogeneous structures in the shock-recovered product but also to the unusually wide mixed-phase region observed in the shock compression curve of forsterite (3, 11).

The fact that the dissociation reaction was not noticed until the peak shock pressure exceeded 80 GPa (4) can be understood if one considers that the reaction kinetics under shock loading is primarily controlled by the shock temperature rather than the pressure. There should be a large discrepancy between the states reached with a single shock in the Hugoniot measurements and those attained with multiple-shock reverberation in the shock recovery experiments, even if the achieved pressure is the same. The temperature increase should be much higher in the former than in the latter case (11).

YASUHIKO SYONO  
TSUNEAKI GOTO  
HUMIHIKO TAKEI

Research Institute for Iron, Steel and  
Other Metals, Tohoku University,  
Sendai 980, Japan

MASAYASU TOKONAMI  
KOHJI NOBUGAI

Institute of Scientific and Industrial  
Research, Osaka University,  
Suita 565, Japan

#### References and Notes

1. T. J. Ahrens, *Science* **207**, 1035 (1980).
2. R. F. Trunin, V. I. Gon'shakova, G. V. Simakov, N. E. Galdin, *Izv. Acad. Sci. USSR Phys. Solid Earth* (1965), p. 1; R. G. McQueen, S. P. Marsh, J. N. Fritz, *J. Geophys. Res.* **72**, 4999 (1967); R. G. McQueen, in *Seismic Coupling*, G. Simmons, Ed. (National Technical Information Service, Springfield, Va., 1968), p. 53; T. J. Ahrens, J. H. Lower, P. L. Lagus, *J. Geophys. Res.* **76**, 518 (1971); G. V. Simakov, M. N. Pavlovskii, N. G. Kalashnikov, R. F. Trunin, *Izv. Acad. Sci. USSR Earth Phys.* (1974), p. 11; R. Jeanloz and T. J. Ahrens, in *High Pressure Research: Applications in Geophysics*, M. H. Manghnani and S. Akimoto, Eds. (Academic Press, New York, 1977), p. 439.
3. I. Jackson and T. J. Ahrens, *J. Geophys. Res.* **84**, 3039 (1979); Y. Syono, T. Goto, J. Sato, H. Takei, *ibid.* **86**, 6181 (1981).
4. R. Jeanloz, *ibid.* **85**, 3163 (1980). Shock metamorphism in olivine has drawn the attention of earth scientists in relation to meteorite impact phenomena. Naturally and experimentally shocked olivines and olivine rocks have been extensively investigated [for instance, W. U. Reimold and D. Stöfler, *Proc. 9th Lunar Planet. Sci. Conf.* (1978), p. 2805]. Shock residual effects in olivine have been less remarkable than those in most silicate minerals, and only a slight indication of the formation of diaplectic glass or recrystallization has been noticed above about 50 GPa [see, for example, R. Jeanloz, T. J. Ahrens, J. S. Lally, G. L. Nord, Jr., J. M. Christie, A. H. Heuer, *Science* **197**, 457 (1977)].

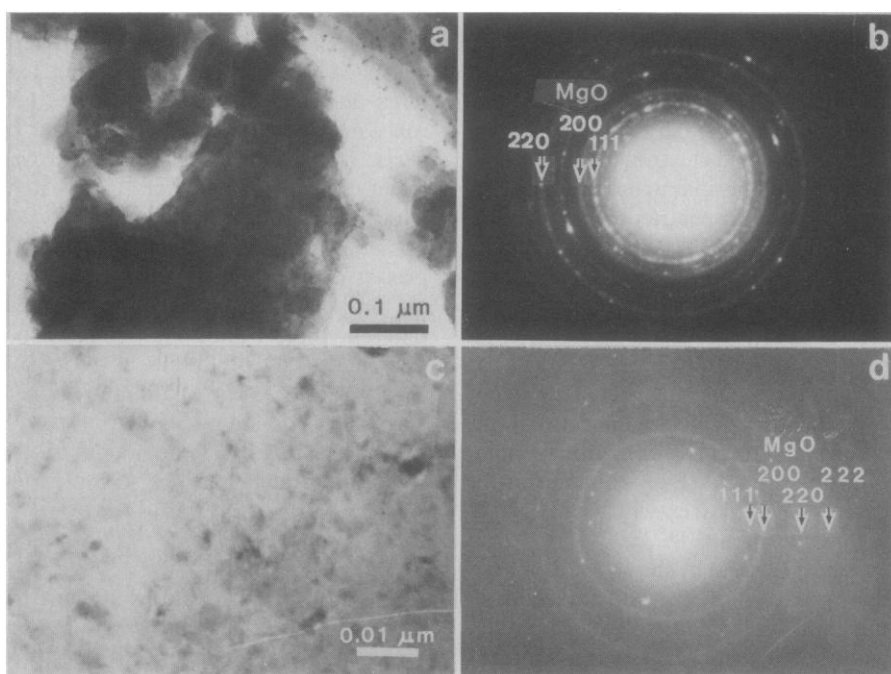


Fig. 2. (a and b) Heterogeneous texture of (010) forsterite shocked to 92 GPa, indicating the coexistence of crystals, recrystallized polycrystalline forsterite, and dissociation product observed under 200-kV TEM. (c and d) Observation with 1000-kV TEM under higher magnification showed that the spherule-like parts of the aggregate as shown in (a) consisted solely of the dissociation assemblage of microcrystalline  $\text{MgO}$  plus glass.

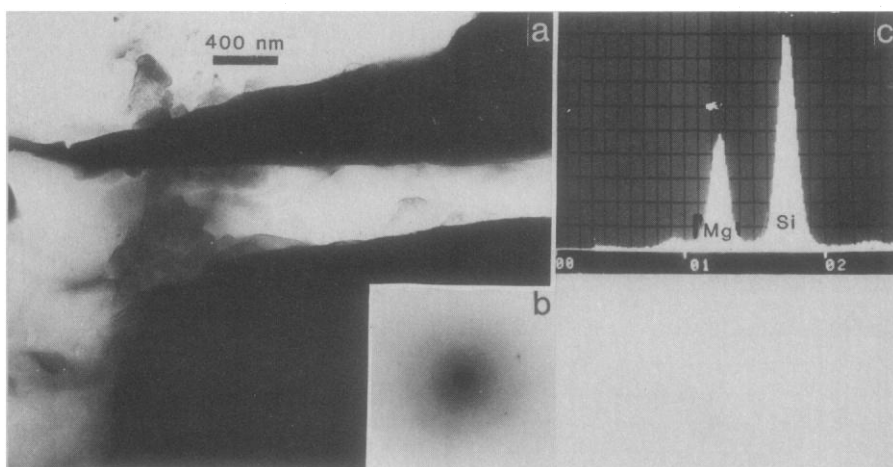


Fig. 3. Differentiated glass in (010) forsterite shocked to 92 GPa: (a) TEM image (100 kV, bright field), (b) electron diffraction pattern, and (c) results of chemical analysis. The Mg/Si ratio of the glass is estimated to be 0.85, in comparison with the peak ratio observed in stoichiometric forsterite (Fig. 1c). This specimen was prepared by ion thinning.

5. Y. Syono and T. Goto, *Sci. Rep. Res. Inst. Tohoku Univ. Ser. A* 29, 17 (1980).
6. H. Takei and T. Kobayashi, *J. Cryst. Growth* 23, 121 (1974).
7. The electron microscopy observations were carried out with 200- and 1000-kV TEM at Tohoku University and 100-kV analytical TEM at Osaka University.
8. L. Liu, *Geophys. Res. Lett.* 2, 417 (1975); *Nature (London)* 262, 770 (1976); E. Ito, *Geophys. Res. Lett.* 4, 72 (1977).
9. Y. Matsui and K. Kawamura, *Nature (London)* 285, 648 (1980); Y. Matsui *et al.*, in *High-Pressure Research in Geophysics*, S. Akimoto and M. H. Manghnani, Eds. (Center for Academic Publications Japan, Tokyo, in press).
10. D. E. Grady, in *High-Pressure Research: Applications in Geophysics*, M. H. Manghnani and S. Akimoto, Eds. (Academic Press, New York, 1977), p. 389.
11. Y. Syono and T. Goto, in *High-Pressure Research in Geophysics*, S. Akimoto and M. H. Manghnani, Eds. (Center for Academic Publications Japan, Tokyo, in press).
12. We benefited from invaluable discussions with Y. Matsui, Okayama University, and I. Kushihiro, University of Tokyo. We thank H. Ohta and E. Aoyagi for technical assistance with the TEM observations and J. Sato and H. Moriya for assistance with preparation of the manuscript. Work supported by Grant in Aid for Special Project Research (321503, 420902, and 510104) given by the Ministry of Education, Science and Culture.

23 March 1981; revised 16 June 1981

## Axonal Transport: Each Major Rate Component Reflects the Movement of Distinct Macromolecular Complexes

**Abstract.** *The proteins of the three major rate components of axonal transport in guinea pig retinal ganglion cells were analyzed by one- and two-dimensional gel electrophoresis. Each rate component consisted of a different set of proteins that remained associated with each other during transport. This suggests that each rate component represents a distinct macromolecular complex and that these complexes may be definable organelles such as microtubules, microfilaments, and smooth endoplasmic reticulum. Thus, the transport of radiolabeled proteins in the axon reflects the movement of complete subcellular structures rather than the movement of individual proteins.*

The axon and its terminal depend on the continuous delivery of proteins synthesized in the cell body to maintain their structural and functional integrity. Axonal proteins leave the cell body as five separate groups, each different and moving at a distinct rate (1-7). Some of these proteins have been associated with specific structures in the axon, such as microtubules, neurofilaments, microfilaments, and mitochondria (2-3, 8). These observations led us to propose a structural hypothesis of axonal transport: proteins are transported in the axon as component parts of intact cytological structures.

Axonal transport was studied in Hartley guinea pig hypoglossal and retinal ganglion cells. The long hypoglossal axons were used to study the kinetics of transport, and the retinal ganglion cell proteins, which could be radiolabeled to high specific activities, were used for more detailed analyses. Transported proteins were labeled by injecting 100 to 500  $\mu\text{Ci}$  of either [ $^{35}\text{S}$ ]methionine or a 1:1 mixture of [ $^3\text{H}$ ]lysine and [ $^3\text{H}$ ]proline into the hypoglossal nucleus or the posterior chamber of the eye (2, 9). At various times thereafter the labeled nerves were removed. The hypoglossal nerve was cut into 3-mm segments, and the radioactive proteins of each rate component of axonal transport were precipitated from the segments with trichloroacetic acid. The polypeptides in each wave were analyzed in segments of

optic nerve and tract by sodium dodecyl sulfate-polyacrylamide gel electrophoresis (SDS-PAGE) alone or in combination with isoelectric focusing (two-dimensional PAGE) (10). Gels were stained with Coomassie blue and radioactive

proteins were detected by fluorography (11).

Three waves of labeled proteins correspond to the major rate components of axonal transport in the hypoglossal nerve (Fig. 1). One wave, present 3 hours after the injection of  $^3\text{H}$ -labeled amino acids, corresponds to the fast component (FC), which moves at about 400 mm/day. Two other waves, one in the proximal portion and one in the distal portion of the nerve 15 days after the injection of  $^3\text{H}$ -labeled amino acids, correspond respectively to slow component a (SCa), moving at 0.3 to 1.0 mm/day, and slow component b (SCb), moving at 2 to 4 mm/day (1, 3, 9). By selecting the injection and analysis intervals appropriately, it is possible to resolve SCa, SCb, and FC from each other and analyze separately the proteins in each rate component. Two other components of axonal transport, which have rates intermediate to those of FC and SCb (6) and represent a much smaller proportion of the total transported radioactivity than that of SCa, SCb, and FC, are not included in this analysis (6, 12).

The SDS-PAGE analyses of SCa, SCb, and FC (Fig. 2) show that most of the radioactive bands are present in just one of the three components (13), but the resolution is insufficient to unequivocally demonstrate that each polypeptide is present in only one rate component. For example, there is an overlap of bands in SCb and FC with molecular weights between 47,000 and 92,000. To resolve these overlapping bands the polypeptides comprising SCa, SCb, and FC were analyzed by two-dimensional PAGE, which separates polypeptides of similar molecular weight by their differences in charge (10). The results (Fig. 3) show that, with only one possible exception [the polypeptide enclosed by parentheses in the fluorographs of SCa and SCb (Fig. 3)], each of the more than 100 polypeptides detected is present in only one rate component. This indicates that SCa, SCb, and FC each consists of distinct polypeptides. Earlier SDS-PAGE studies (1-3, 8) showed that different polypeptides are transported at each of the five rates but did not reveal the distinctive composition of each rate component. The pattern of spots produced by two-dimensional PAGE (Fig. 3) may be used to identify and rigorously define the protein composition of each rate component.

Any model to explain axonal transport must now account for the segregation of the proteins in one rate component apart from those in other rate components as they move past one another. Some cur-

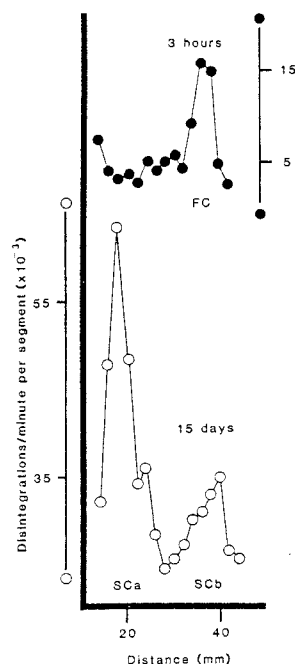


Fig. 1. The distribution of radioactive proteins in the hypoglossal nerves of two guinea pigs 3 hours or 15 days after an injection of  $^3\text{H}$ -labeled amino acids. The scale of disintegrations per minute per segment is on the right for FC and on the left for SCa and SCb. The distance is measured from the hypoglossal nucleus.